ISSN 1330-3651(Print), ISSN 1848-6339 (Online) https://doi.org/10.17559/TV-20240725001880
Original scientific paper

Experimental and Numerical Investigation of the Plastic Region Behaviours of AA 1100 and AA 7075 Aluminium Alloys at Different Velocities and Energy Levels

Onur GÖK, Mehmet KAYRICI, Mehmet Turan DEMİRCİ

Abstract: This study investigated the Johnson-Cook (J-C) plastic region model of AA-1100 and AA-7075 series aluminium alloys. The tensile, three-point bending and low-velocity impact strengths at different velocities were investigated by keeping the equation constants and temperature constant for the J-C plastic region structural model. Tensile tests and three-point bending tests were performed at velocities of 1, 10, 20, and 40 s^{-1}, respectively. Low-velocity impact tests of AA-1100 and AA-7075 alloys were performed at energy levels of 33,35, 66,71, 100, and 133,42 J, corresponding to velocities of 1,98(0.2 m), 2,80(0.4 m), 3,43(0.6 m) and 3,96(0.8 m) m/s, respectively. In addition, the materials' three-point bending, and low-velocity impact responses were also numerically investigated using a finite element model and compared with the experimental results. It is observed that the experimental and numerical results are in agreement with each other.
Keywords: AA-1100; AA-7075; Finite Element Method; Plastic Deformation; Johnson-Cook

1 INTRODUCTION

Aluminium and its alloys are widely used in engineering, aerospace, transportation, defense, and medical fields. These alloys are essential in engineering due to their light weight, durability, and ease of manufacturing processes. For these reasons, the mechanical behavior of aluminum alloys is critical in materials science. The mechanical properties of aluminum alloys vary according to the material composition, production method, and heat treatment of the alloy [1-3]. Many experimental methods are used to determine the mechanical behavior of materials. These methods determine the mechanical properties of ductile metal materials. It is possible to classify mechanical behavior as elastic, plastic, and fracture behavior with these tests. As a result of these tests, it is possible to model the materials mathematically and explain the material behavior for elastic and plastic regions with mathematical values [4].

Many material models are used mathematically to explain the plastic behavior of materials. Some are Zener-Hollomon, Johnson-Cook (J-C), and Zerilli-Armstrong (Z-A) material models. Mathematically modeling the plastic region behavior of materials is very important for design optimization in engineering designs before manufacturing processes. The J-C material model, used in recent years to make these optimizations, is one of these material models [5-8]. The J-C material model is generally used to predict the dynamic behavior of materials. These dynamic behaviors are collision, interference, and plastic deformation behaviors, and explaining these behaviors is very important in engineering design. Determining the mechanical behavior of a material by experimental methods is an expensive and time-consuming process. The necessity of experimental methods is indisputable, but the mechanical properties determined should be used in the design phase without going through the manufacturing stages for the engineered product. Eliminating these processes will enable the product to be produced in shorter times and at very low costs. In this way, financial losses will be minimized. However, before performing such an optimization study, experimental and numerical results should be compared and verified [9]. There are studies on this model in the literature. In these studies, the strain hardening effect was significant in AA-7075-T6 in tensile tests at high strain rates. The J-C material model can accurately reflect the mechanical properties of AA-7075-T6 under different strain rates. For AA-7050-T-7451, the proposed Modified Johnson-Cook (M-J-C) model to describe the plastic region behavior based on strain hardening coefficient at various strain rates gave better results compared to Khan-Liv (K-L) model J-C model. As a result, it was determined that the J-C material model makes it possible to predict aluminum alloy's plastic region stress behavior [2, 10]. In another study, Z-A and Arhenius-type models were used to indicate the plastic region stresses of AA-7050 alloy at high temperatures. Both models predicted the plastic region stress behavior of AA-7050 alloy with higher accuracy. However, it was concluded that the combined deformation-temperature effect is weak in predicting the plastic region stress behavior of AA-7050 alloy [11]. High-velocity tensile testing machines and Split Hopkinson Bar (SPHB) machines apply high-velocity forming processes to aluminum alloys. In another study, high-velocity tensile testing was performed electro-magnetically, the material was tested electro-magnetically at high strain rates, and the results matched the results obtained by conventional test methods. [12].

Finite element simulations determined the surface stresses and stress-strain states of rolled AA-5083-O alloy sheet material at different stresses. J-C fracture criteria were applied as a user-defined function to the ABAQUS package program to determine the fracture initiation, and it was concluded that the experimental and numerical results were compatible [13]. The results obtained from SHPB experiments at high temperatures for AA-7017 alloy were applied to the J-C model, and it was concluded that this model can predict the plastic region stress of the alloy under various strains and temperatures [14, 15]. The hot deformation behavior of AA-7055 sputtered alloy was investigated by hot compression tests with three material models: J-C, Field-Bakofen (F-B), and Arrhenius type. Arrhenius material model was found to provide the best fit by combining strain rate and temperature effects [16]. The yield region and fracture behavior of AA-7075 T-651 alloy was investigated quasi-statically under different stresses, strain rates, and temperatures. The linear decrease of the modulus of elasticity with increasing temperature was observed, and it was seen that the J-C material model could

accurately describe the penetration behavior and ballistic resistance in the ballistic test results.

The best ductility and strain hardening effect was found at 200 ºC in studies carried out between 25-250 ºC to determine the hot formability of AA-7075-T6 alloy and the microstructure-strength relationship after treatment [17, 18]. The J-C material model has been applied in mathematical calculations with many finite element methods. However, the prediction accuracy of the original J-C model is limited by considering the extensive influence of temperatures, stresses, and strain rates on the plastic region behavior of materials. [19]. Therefore, the mathematical model has been revised several times by considering the effect of adiabatic temperature rise and strain rate sensitivity during material deformation [7, 20]. In another study, the ballistic behavior of thin shells was investigated using the J-C model in the finite element package program ABAQUS-EXPLICIT. It was found that the ballistic limit of AA-7075 alloy was the highest, and the ballistic limit of AA-1100 alloy was the lowest. It was observed that the strain hardening effect for AA-1100 alloy was similar at quasi-static strain rates at room temperature, and the J-C model was consistent with experimental studies and finite element analysis [21, 22]. The study by Johnson GR et al. showed that the J-C material model can produce results that are exceptionally compatible with experimental results in ductile materials. As a result of the sources researched, J-C, Z-A, Arrhenius, Voyiadjis-Abed (V-A) Model, Preston-Tonk-Wallace (P-T-W) Model, Khan-Huang-Liang (K-H-L) Model, Gao-Zhang (G-Z) Model type material models are examples of mathematical models commonly used in numerical simulation [8, 23, 24]. In the studies, it can be generally said that plastic material models can describe the strain-hardening effect and experimental results in both aluminum alloys and steels.

Regarding the studies conducted in this context, AA-1100 and AA-7075 alloys were preferred, and the Johnson-Cook plastic region model was investigated at different tensile velocities. Thus, the results of tensile tests performed at different tensile velocities of 1, 10, 20, and 40 s^{-1} and low-velocity impact tests applied within the scope of varying energy levels were compared dynamically and numerically with the finite element method.

2 EXPERIMENTAL AND NUMERIC ANALYSIS

To characterize the plastic region response of AA-1100 and 7075 sheet metal alloys, uniaxial tensile, low-velocity impact, and three-point bending tests were carried out at room temperature conditions. The finite element method was also used as a numerical method. The chemical compositions of AA-1100 and AA-7075 alloys used in the experimental studies are given in Table 1, respectively. Macro images of aluminum and alloys prepared for the experiments are given in Figure 1.

Tensile test specimens were prepared according to the ASTM 8E standard, low-velocity impact test specimens according to the ASTM D7136 standard, and three-point bending test specimens according to the ASTM D790 standard. These specimens were cut with a precision CNC milling machine using coolant from a sheet metal plate parallel to the rolling direction to the dimensions shown in Figure 1 for AA-1100 and AA-7075 alloys.

Table 1 The chemical composition of materials

AA-1100		AA-7075	
Element Name	wt. %	Element Name	wt. %
P	0,01	Si	0,07
Ca	0,05	Fe	0,12
Si	0,6	Cu	1,5
Ga	0,02	Mn	0,02
Mg	0,09	Cr	0,18
Fe	0,55	Zn	5,8
Al	98,66	Ti	0,05

The specimens were subjected to tensile tests at velocities of 1, 10, 20, and 40 s^{-1}, respectively, as shown in Figure 2. The specimens were anchored to the upper and lower jaws, and the tensile test was continued along the +y axis, with the movement of the upper jaw at one degree of freedom until the specimen broke.

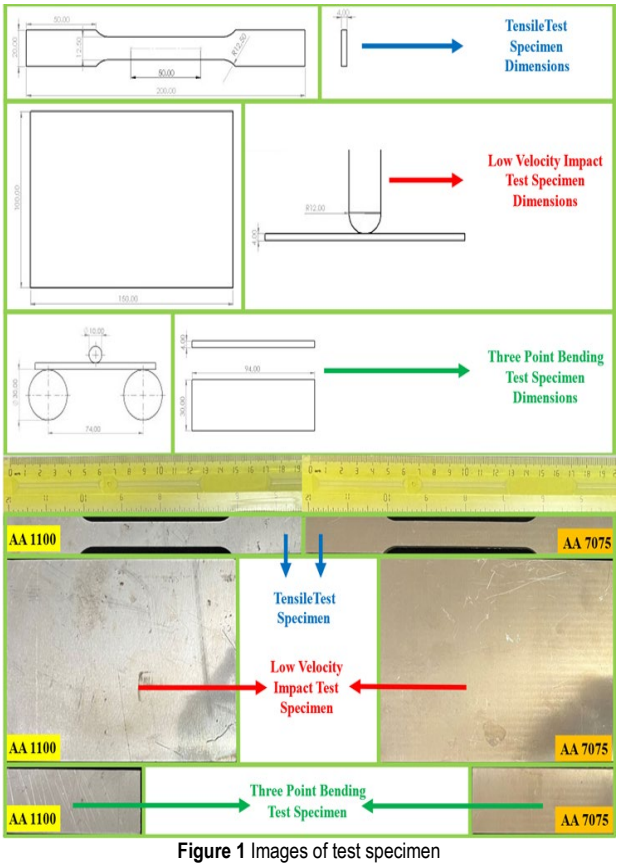

Figure 1 Images of test specimen

The specimens prepared for low-velocity impact testing were subjected to low-velocity impact tests at energy-height levels of 0,2 m (1,98 m/s, 33,35 j), 0,4 m (2,80 m/s, 66,71 j), 0,6 m (3,43 m/s, 100 j) and 0,8 m (3,96 m/s, 133,42 j). Figure 3 shows the impact testing machine used. This device initiated the application process with a free fall movement by bringing a 17 kg mass, called the striking mass, to a fixed height at the desired energy level value. With this free fall movement, the impact process was carried out in specially prepared specimen moulds for the specimens. In the specimens connected to the mould, it was ensured to be as anchored as possible with screws tightened at equal torques for the specimen surfaces. Figure 3 shows the degree of freedom of the specimen and the striking mass. While the striking mass made a free fall movement, all other degrees of freedom were restricted due to the construction structure

of the low-velocity impact test device, and the movement was realized only in the -y direction.

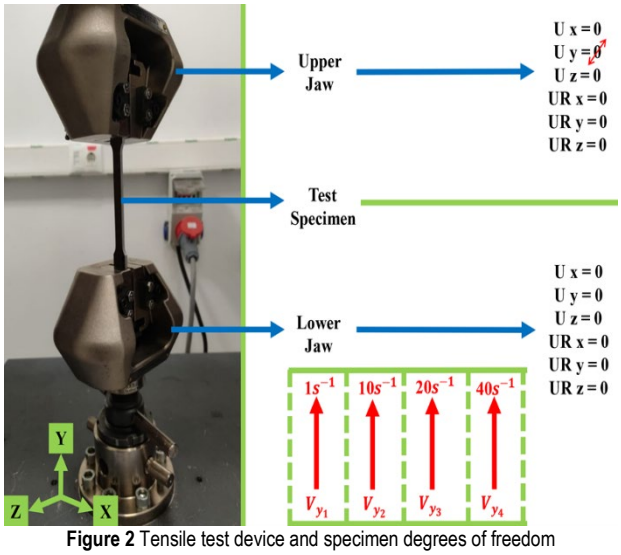

Figure 2 Tensile test device and specimen degrees of freedom

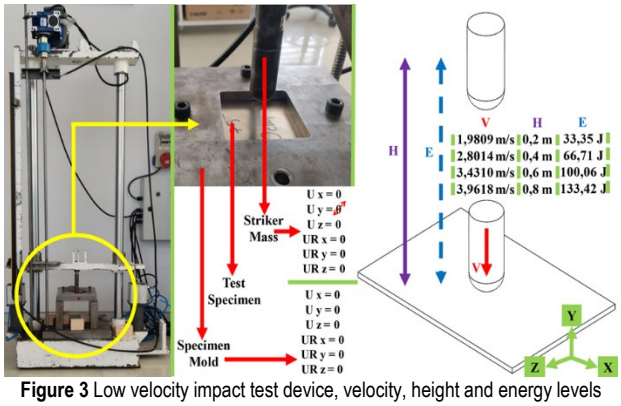

Figure 3 Low velocity impact test device, velocity, height and energy levels

For three-point bending tests, flexure test specimens prepared according to ASTM D790 were subjected to the test at velocities of 1, 10, 20 and 40 s^{-1} respectively. The test was continued by moving the striking mass along the -y until the specimen fell or fractured from the support points in Figure 4.

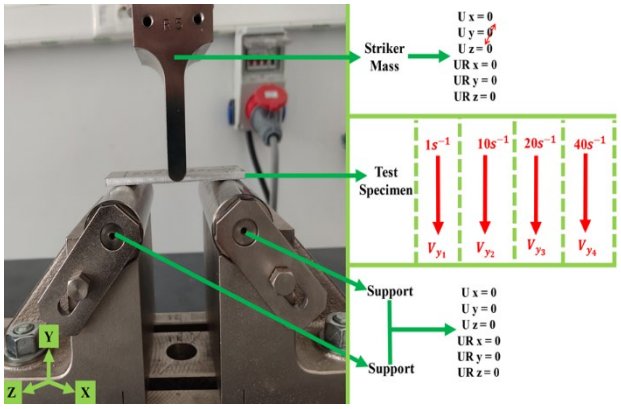

Figure 4 Three-point bending test device and degrees of freedom

The stages of this process are the creation of the CAD geometry, the creation of the mathematical model, the application of boundary conditions by the analysis model characteristics, and finally, the analysis of the results. The boundary conditions applied for the finite element analysis are shown in Figure 5 for the low-velocity impact calculation. Rotational and translational motions along all axes of the anchored surfaces are assumed to equal zero. The degree of freedom of the striking mass is supposed to be one. While the three rotational motions are considered zero, the translational motion in the drop axis is left free. This definition is used to define the free movement of the striking mass along the axis of fall in the mathematical model. The striker mass was considered rigid, and the analysis was run with an explicit solver. A total of 45840 elements were used in the analysis. The CAD model was converted into a mathematical model using C3D8R elements, and the mathematical model was converted into a network structure. For finite element analysis, ¼ symmetry was used in model definition.

The striker mass was considered rigid, and a three-point bending analysis was run with ABAQUS EXPLICIT SOLVER. A total of 22200 elements were used in the analysis. The CAD model was converted into a mathematical model using C3D8R elements, and the mathematical model was converted into a mesh structure. It was not used in the model definition for finite element analysis. The boundary conditions applied for finite element analysis are shown in Figure 5 for low-velocity impact three-point bending calculation. Rotational and translational motions along all axes of the anchored surfaces are assumed to equal zero. The degree of freedom of the striking mass is supposed to be one. While the three rotational motions are considered zero, the translational motion in the drop axis is left free. This definition is used to define the free movement of the striking mass along the axis of fall in the mathematical model.

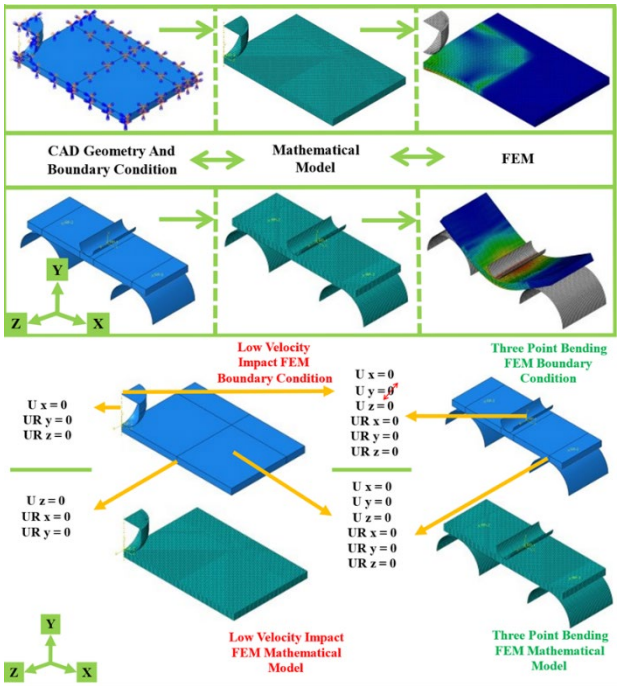

Figure 5 Low velocity impact test finite element boundary condition and model mesh structure

In the study, the finite element method did not define displacement progression and velocity changes taken from

experimental data. One of the biggest mistakes was defining the experiments' process data using the finite element method. In this case, it shows animation behavior rather than simulation. The correct way is to define a constant velocity for the striking mass in advance and leave the calculation to the solver. In this study, experimental data was not defined in the program. It is left to the solver's calculation and to stop the striker due to the rigidity of the AA alloys.

3 RESULTS AND DISCUSSION

The tensile macrostructure images of the fracture surface of AA-1100 and AA-7075 aluminum alloys are shown in Figure 6. When the rupture surface macrostructure images are examined, it can be seen that the fracture morphology of AA-7075 alloy is more brittle compared to the necking observed in AA-1100 alloy. The actual stress-strain curves obtained for AA-1100 and AA-7075 materials as a result of the tensile test at different velocities are shown in Figure 6 as a single figure to more clearly indicate the mechanical behavior of the materials and the difference in mechanical behavior between the two different aluminum alloys.

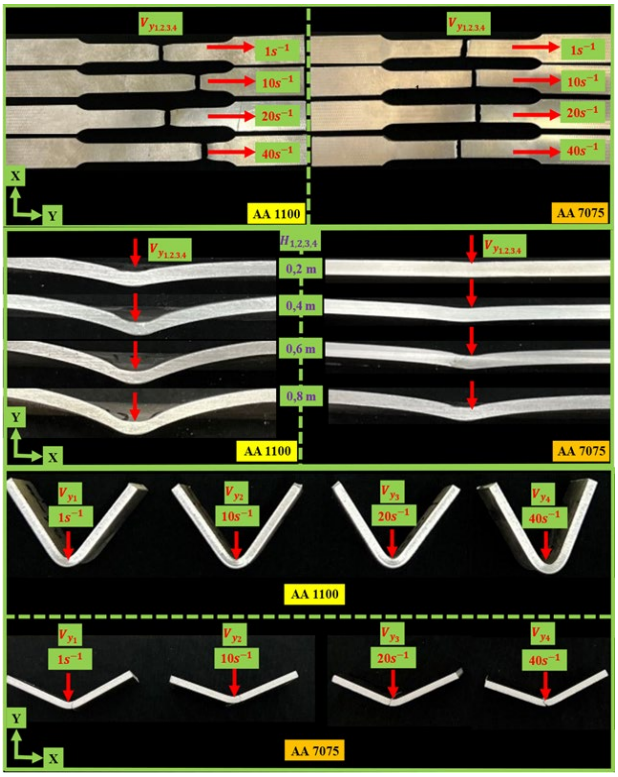

Figure 6 AA-1100 and AA-7075 alloy tensile, low velocity impact, three point bending test macro structure images

As a result of the low-velocity impact tests, the visual results obtained from the impact tests at heights of 0,2 m (1,98 m/s, 33,35 j), 0,4 m (2,80 m/s, 66,71 j), 0,6 m (3,43 m/s, 100 j) and 0,8 m (3,96 m/s, 133,42 j) are given in Figure 6 for AA-1100 alloy and AA-7075 alloy.

As a result of the three-point bending test three-point bending visual results for the AA-1100 and AA-7075 alloys are shown in Figure 6. The maximum force obtained for AA-1100 alloy was 1 180 N for 1 s^{-1}, 1 200 N for 10 s^{-1}, 1 240 N for 20 s^{-1}, and 1 310 N for 40 s^{-1} according to the bending test velocities. The maximum force obtained for AA-7075 alloys was 6 170 N for 1 s-1, 6 250 N for 10 s^{-1}, 6 310 N for 20 s^{-1}, and 6 400 N for 40 s^{-1} according to bending test velocities, as seen in the graphs in Figure 7.

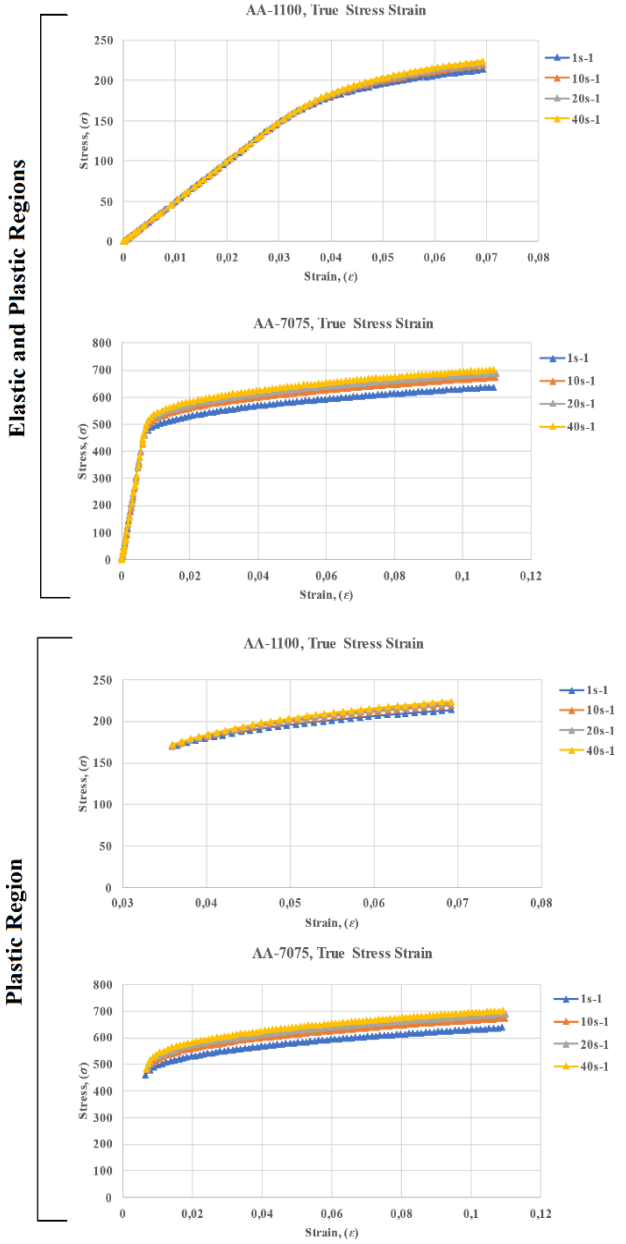

Figure 7 True stress-strain curve of AA-1100 and AA-7075 alloys

To determine the constants A, B, and n, the general J-C equation in equation 1 is reduced to equation 2.

$$\sigma = (A + B\varepsilon^{n}) \times (1 + C\, ln\, \dot{\varepsilon}^{*}) \times (1 + T^{*m}) \quad (1)$$

$$\sigma = A + B\varepsilon^{n} \quad (2)$$

After this process, the coefficient A, representing the yield point in equation 2, can be subtracted from the plastic stress values. Then, the natural logarithm of both sides is changed from a parabolic function to a linear function, and equation 3 is obtained.

$$ln(\sigma - A) = ln\, B + n\, ln\, \varepsilon \quad (3)$$

The coefficients A, B, and n were found, as shown in Figure 8, by regression analysis of this equation and the plastic region graph obtained at 1 s^{-1} tensile velocity. Then, to determine the C constant, the A, B, and n coefficients obtained in the equation were substituted, and the C constant was obtained by taking the natural logarithm of both sides to obtain Equations 4 and 5.

$$\sigma = (A + B\varepsilon^n)(1 + C\, ln\, \dot{\varepsilon}^*) \quad (4)$$

$$\frac{\sigma}{A+B\varepsilon^n} - 1 = C\, ln\, \dot{\varepsilon}^* \quad (5)$$

In this way, the C coefficient is calculated with the data obtained from tensile tests at 10, 20, and 40 s^{-1}, and the slope of the line by regression method gives us the C constant. The graph of the C constant is shown in Figure 8. The process steps applied for AA-1100 material were used for AA-7075, and the coefficients A, B, and n and C constant were obtained by regression method as shown in Figure 8. As a result of the tensile tests and calculation of J-C plastic deformation region constants, the material mechanical properties obtained for AA-1100 and AA-7075 aluminum alloys are given in Table 2.

Table 2 Calculated J-C plastic region material constants

Constant	AA-1100	AA-7075
E	5 250	71 700
υ	0,33	0,33
A	106	460
B	222	571
n	0,2	0,42
C	0,02	0,003

As a result of the low-velocity impact tests, the low-velocity impact test for AA-7075 alloy and the numerical results calculated for this alloy are given as a cross-sectional view in Figure 9. Although it is a dynamic test, it is observed that the plastic region deformations after the impact are experimentally and numerically compatible with each other. Still, the amount of compliance decreases slightly as the impact energy levels increase. Unlike the AA-1100 alloy, it is observed that the AA-7075 alloy does not give as close results as the AA-1100 alloy in the first place, as seen by looking at the experimental and numerical analysis results in visual findings.

As a result of the finite element model calculated as a continuation of the experimental studies, impact test calculations were made at heights of 0,2 m (1,98 m/s, 33,35 j), 0.4 m (2,80 m/s, 66,71 j), 0,6 m (3,43 m/s, 100 j) and 0,8 m (3,96 m/s, 133,42 j). The visual results obtained for the J-C plastic region AA7075 alloy calculated as a result of tensile tests at different velocities, the cross-sectional front view, and the low-velocity impact test results with isometric cross-sectional structural model constants are given comparatively for AA-1100 and AA-7075 alloys Figure 9.

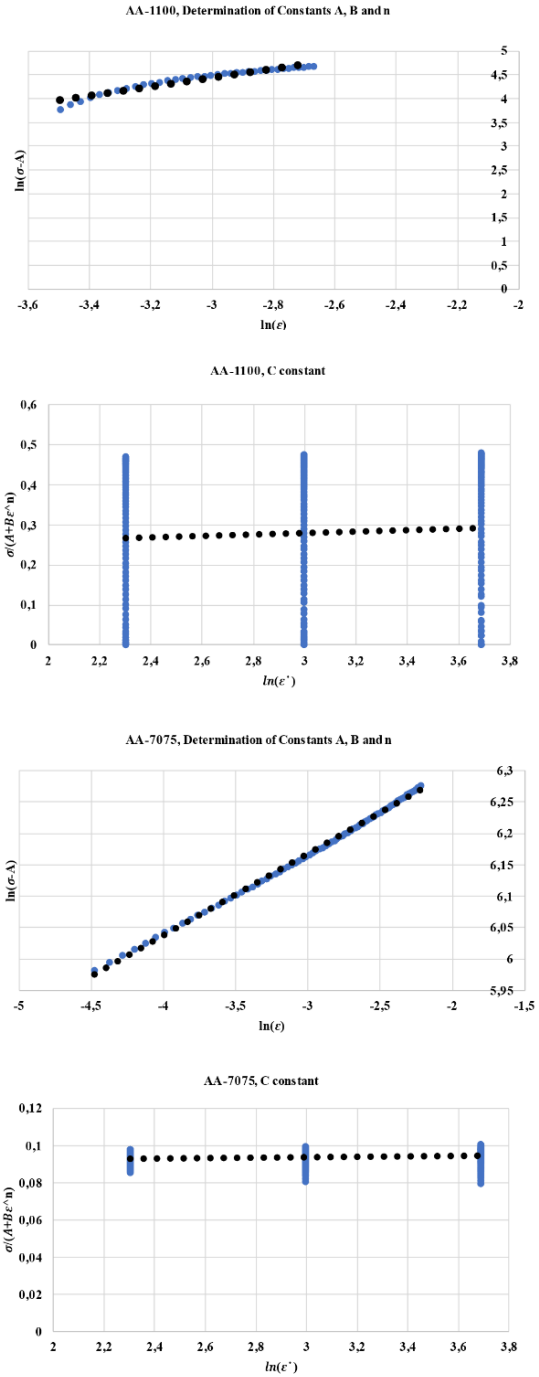

Figure 8 Determination of AA-1100, AA-7075 alloy A, B, n coefficients and c constants

Although it is a dynamic test, it is observed that the plastic region deformations after the impact are experimentally and numerically consistent with each other. Still, the amount of agreement decreases slightly as the impact energy levels increase. The force-time, force-displacement, and energy-time plots for all energy levels are given in Figure 10, respectively. The maximum force values for different energy levels in the force-time curves for AA-1100 alloy were found as 0,2 m- 8 480 N, 0,4 m- 11 150 N, 0,6 m – 14 380 N, and 16 550 N for 0,8 m energy level. When the force-displacement curves are analysed, the displacement value corresponding to 0,2 m- 8 480 N is 0,0062 m, the displacement value corresponding to 0,4 m – 11 150 N is 0,0094 m, the displacement value

corresponding to 0,6 m – 14 380 N is 0,013 m and the displacement value corresponding to 0,8 m – 16 550 N is 0,01496 m.

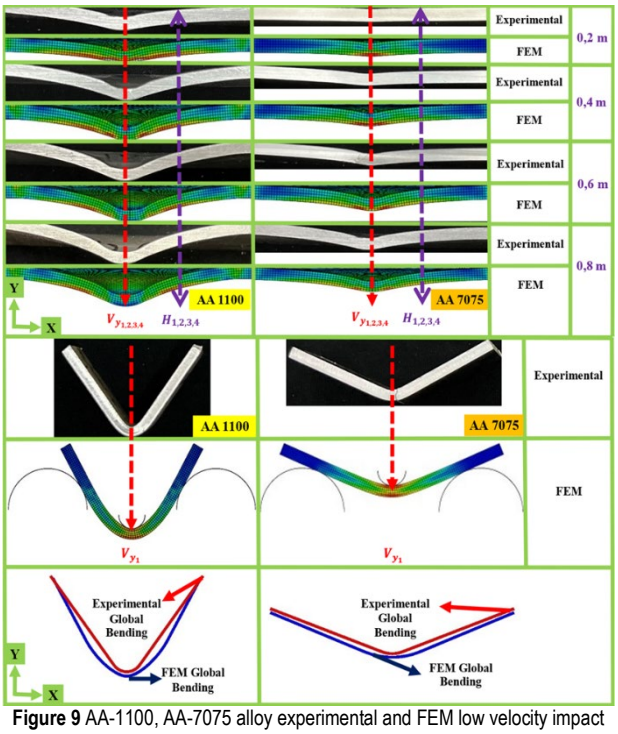

Figure 9 AA-1100, AA-7075 alloy experimental and FEM low velocity impact and three point bending test image

The force-time, force-displacement, and energy-time graphs for all energy levels are shown in Figure 10, respectively. When the force-time curves obtained for AA-7075 alloy are examined, the maximum force values for different energy levels are determined as 0,2m- 17 110 N, 0,4 m- 23 350 N, 0,6 m- 27 130 N and 31 700 N for 0,8 m energy level, respectively. In the force-displacement curves, the displacement value corresponding to 0,2m – 17 110 N was 0,0033 m, 0,4 m- 23 350 N was 0,0049 m, 0,6 m- 27 130 N was 0,00671 m and 0,8 m- 31 700 N was 0,0081 m. 0,2 m striker height is the minimum height at which visible damage occurs.

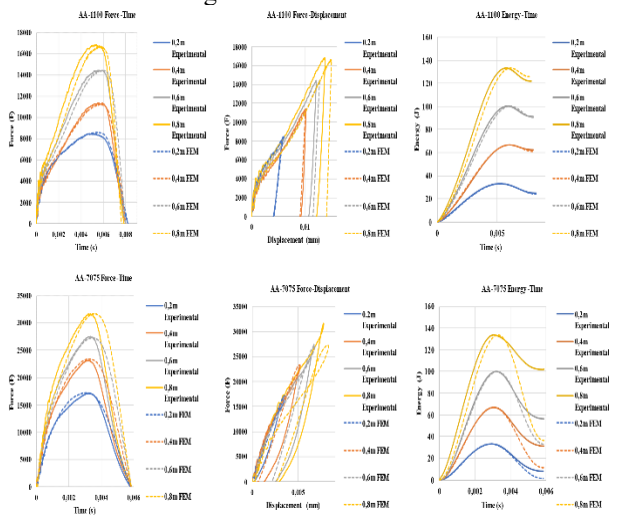

Figure 10 AA-1100, AA-7075 alloy experimental and FEM low velocity impact; force-time, force-displacement and energy-time curves

Macro images of AA-1100 and AA-7075 alloys after three-point bending tests are shown in Figure 12. In the finite element model created for three-point bending tests, model calculations were made for 1 s-1, and finite element images are given in Figure 11 for AA-1100 and AA-7075 alloys. Three-point bending and low-velocity impact tests performed with the J-C plastic region structural model constants calculated as a result of tensile tests at different velocities were examined experimentally and numerically in a comparative manner. Three-point bending tests are given for AA-1100 and AA-7075 alloys— Figure 11.

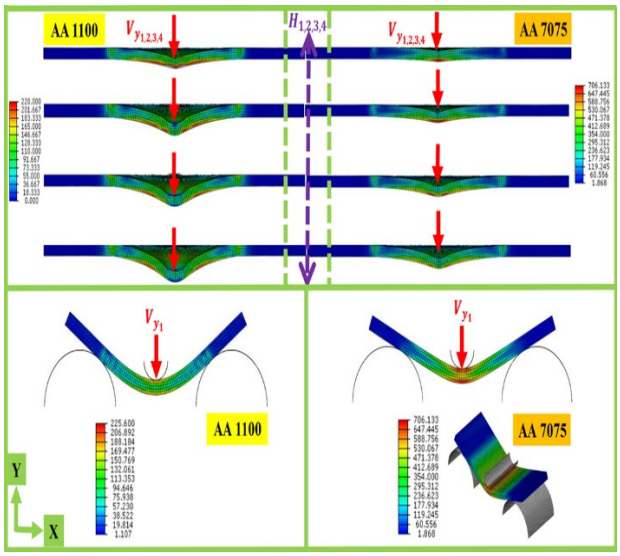

Figure 11 FEM three-point bending test results of specimen

The force-extension graphs obtained after the bending test of aluminum alloys are shown in Figure 12 for elastic and plastic regions. For the J-C model, speeds of 1 s-1, 10 s-1, 20 s-1, and 40 s-1 were selected to determine the flexural behavior under dynamic velocity. The maximum force obtained for AA-1100 alloy was 1 180 N for 1 s^{-1}, 1 200 N for 10 s^{-1}, 1 240 N for 20 s^{-1}, and 1 310 N for 40 s^{-1} according to the bending test velocities. For A-7075 alloy, the maximum force was 6 170 N for 1 s^{-1}, 6 250 N for 10 s^{-1}, 6 310 N for 20 s^{-1}, and 6 400 N for 40 s^{-1} according to the bending test velocities. The force strain graphs obtained for aluminum alloys are compared with the experimental data, and the comparative graphs with the numerical data calculated for 1 s^{-1} are given in Figure 12. When the three-point bending test results given in Figure 12 for aluminum alloys are examined, the elastic region shows complete agreement in the graph. In contrast, the deal in the plastic region is very close to the experimental data. This agreement is because the velocity used in the three-point bending test is low, and the alloys' coarsening exponent is found correctly.

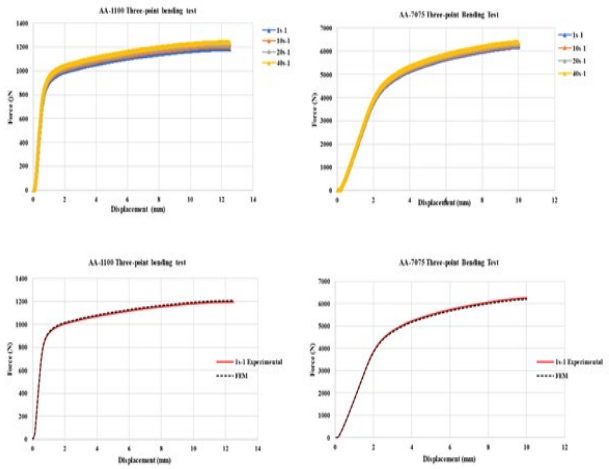

Figure 12 Three-point bending test experimental results of specimen

4 CONCLUSIONS

In this study, where the tensile and low-velocity impact behaviors of AA-1100 and AA-7075 aluminum alloys at different velocities and energy levels were investigated experimentally and numerically, the following results were obtained;

- The modulus of elasticity for A-1100 alloy varies between 67 000 MPa-71 000 MPa in the literature. Unlike the literature, the modulus of elasticity of AA-1100 alloy was determined as 5 200 MPa.

- J-C constants for AA-1100 and AA-7075 alloys after tensile tests were found to be different from the literature.

- Although the C constant, the strain sensitivity for AA-1100 alloy, was found to be 0,001 in the literature, the regression coefficients were calculated as 0,99 in the experimental results obtained, and the C constant was found to be 0,02.

- In the tensile tests performed at different velocities, the tensile strength change, which is the maximum strength value of AA-1100 alloy changing against the tensile velocity, has entered a more pronounced change than AA-7075 alloy.

- According to the results of the low-velocity impact test with the calculated J-C model constants. However, dynamic behavior modeling for AA-1100 alloy is very close to the numerical calculation and experiment. Rather than the values obtained in the graphs, the graphical characteristics show very close behavior to each other. For the plastic region behavior of the alloy, the experimental and numerical results were close to each other. However, the agreement of AA-7075 alloy with numerical results was lower in AA-1100 alloy.

- The J-C material model was correctly defined for the global bending regions given visually by three-point bending tests and showed high similarity with the numerical results. For low-velocity impact tests, which are dynamic tests, when global bending and local bending were examined together in this study, both local and global bending deformations for AA-1100 alloy were highly compatible with numerical calculation. In contrast, global bending deformation in AA-7075 alloy was very compatible with numerical calculation, but local bending in strain hardening region was less compatible than AA-1100 alloy.

- It is concluded that J-C plastic material model constants better describe the dynamic behavior of unalloyed pure ductile metals and give more accurate convergence than alloyed materials.

Acknowledgements

This study is derived from his Ph.D. thesis, Investigation of the plastic region behavior of 7075 and 1100 series aluminum alloys. No project or financial support was received for this study.

5 REFERENCES (According to APA)

[1] Abotula, S., Shukla, A., & Chona, R. (2011). Dynamic constitutive behaviour of Hastelloy X under thermo-mechanical loads. Journal of Materials Science, 46, 4971–4979. https://doi.org/10.1007/s10853-011-5414-y

[2] Huh, H., Lee, H. J., & Song, J. H. (2012). Dynamic hardening equation of the auto-body steel sheet with the variation of temperature. International Journal of Automotive Technology, 13, 43–60. https://doi.org/10.1007/s12239-012-0005-8

[3] Zhang, D.-N., Shangguan, Q.-Q., Xie, C.-J., & Liu, F. (2015). A modified Johnson–Cook model of dynamic tensile behaviors for 7075-T6 aluminum alloy. Journal of Alloys and Compounds, 619, 186–194. https://doi.org/10.1016/j.jallcom.2014.09.002

[4] Dehgolan, F. R., Behzadi, M., & Sola, J. F. (2016). Obtaining constants of Johnson-Cook material model using a combined experimental, numerical simulation and optimization method. Int. J. Mech. Mechatron. Eng, 33, 1615–1622.

[5] Johnson, G. R. (1983). A constitutive model and data for metals subjected to large strains, high strain rates and high temperatures. In Proceedings of the 7th International Symposium on Ballistics, The Hague, Netherlands, 1983

[6] Xue, L., & Wierzbicki, T. (2009). Ductile fracture characterization of aluminium alloy 2024-T351 using damage plasticity theory. International Journal of Applied Mechanics, 1(02), 267–304. https://doi.org/10.1142/S1758825109000198

[7] Lin, Y. C., Chen, X.-M., & Liu, G. (2010). A modified Johnson–Cook model for tensile behaviours of typical high-strength alloy steel. Materials Science and Engineering: A, 527(26), 6980–6986. https://doi.org/10.1016/j.msea.2010.07.061

[8] Johnson, G. R., & Cook, W. H. (1985). Fracture characteristics of three metals subjected to various strains, strain rates, temperatures and pressures. Engineering fracture mechanics, 21(1), 31-48. https://doi.org/10.1016/0013-7944(85)90052-9

[9] Farahani, H. K., Ketabchi, M., & Zangeneh, S. (2017). Determination of Johnson–Cook plasticity model parameters for Inconel718. Journal of Materials Engineering and Performance, 26, 5284–5293. https://doi.org/10.1007/s11665-017-2990-2

[10] Tan, J. Q., Zhan, M., Liu, S., Huang, T., Guo, J., & Yang, H. (2015). A modified Johnson–Cook model for tensile flow behaviours of 7050-T7451 aluminium alloy at high strain rates. Materials Science and Engineering: A, 631, 214–219. https://doi.org/10.1016/j.msea.2015.02.010

[11] Li, J., Li, F., Cai, J., Wang, R., Yuan, Z., & Ji, G. (2013). Comparative investigation on the modified Zerilli–

Armstrong model and Arrhenius-type model to predict the elevated-temperature flow behaviour of 7050 aluminium alloy. Computational Materials Science, 71, 56–65. https://doi.org/10.1016/j.commatsci.2013.01.010

[12] Deng, H., Yang, S., Li, G., Zhang, X., & Cui, J. (2020). Novel method for testing the high strain rate tensile behaviour of aluminium alloys. Journal of Materials Processing Technology, 280, 116601. https://doi.org/10.1016/j.jmatprotec.2020.116601

[13] Qian, L.-Y., Fang, G., Zeng, P., & Wang, Q. (2015). Experimental and numerical investigations into the ductile fracture during the forming of flat-rolled 5083-O aluminium alloy sheet. Journal of Materials Processing Technology, 220, 264–275. https://doi.org/10.1016/j.jmatprotec.2015.01.031

[14] Karkalos, N. E., & Markopoulos, A. P. (2018). Determination of Johnson-Cook material model parameters by an optimization approach using the fireworks algorithm. Procedia Manufacturing, 22, 107–113. https://doi.org/10.1016/j.promfg.2018.03.017

[15] Bobbili, R., Ramakrishna, B., Madhu, V., & Gogia, A. K. (2015). Prediction of flow stress of 7017 aluminium alloy under high strain rate compression at elevated temperatures. Defence Technology, 11(1), 93–98. https://doi.org/10.1016/j.dt.2014.08.004

[16] Wang, X., Pan, Q., Xiong, S., Liu, L., Sun, Y., & Wang, W. (2018). Prediction on hot deformation behaviour of spray-formed 7055 aluminium alloy via phenomenological models. Transactions of Nonferrous Metals Society of China, 28(8), 1484–1494. https://doi.org/10.1016/S1003-6326(18)64789-2

[17] Senthil, K., Iqbal, M. A., Chandel, P. S., & Gupta, N. K. (2017). Study of the constitutive behaviour of 7075-T651 aluminium alloy. International Journal of Impact Engineering, 108, 171–190. https://doi.org/10.1016/j.ijimpeng.2017.05.002

[18] Huo, W., Hou, L., Zhang, Y., & Zhang, J. (2016). Warm formability and post-forming microstructure/property of high-strength AA 7075-T6 Al alloy. Materials Science and Engineering: A, 675, 44–54. https://doi.org/10.1016/j.msea.2016.08.054

[19] Gupta, A. K., Anirudh, V. K., & Singh, S. K. (2013). Constitutive models to predict flow stress in Austenitic Stainless Steel 316 at elevated temperatures. Materials & Design, 43, 410–418. https://doi.org/10.1016/j.matdes.2012.07.008

[20] Wang, Y., Zhou, Y., & Xia, Y. (2004). A constitutive description of tensile behavior for brass over a wide range of strain rates. Materials Science and Engineering: A, 372(1–2), 186–190. https://doi.org/10.1016/j.msea.2003.12.009

[21] Khaire, N., Tiwari, G., & Gurusankar, A. (2020). Numerical study of energy absorption behaviour of thin aluminium hemispherical shell against projectile impact. Materials Today: Proceedings, 21, 1958–1963. https://doi.org/10.1016/j.matpr.2020.01.281

[22] Sahu, S., Mondal, D. P., Goel, M. D., & Ansari, M. Z. (2018). Finite element analysis of AA1100 elasto-plastic behaviour using Johnson-Cook model. Materials Today: Proceedings, 5(2), 5349–5353. https://doi.org/10.1016/j.matpr.2017.12.120

[23] Zerilli, F. J., & Armstrong, R. W. (1987). Dislocation-mechanics-based constitutive relations for material dynamics calculations. Journal of Applied Physics, 61(5), 1816–1825. https://doi.org/10.1063/1.338024

[24] Sellars, C. M., & McTegart, W. J. (1966). On the mechanism of hot deformation. Acta Metallurgica, 14(9), 1136–1138. https://doi.org/10.1016/0001-6160(66)90207-0

Contact information:

Onur GÖK, Lecturer PhD.
(Corresponding author)
Necmettin Erbakan University, Seydişehir Vocational Scholl
Prof. Dr. Necmettin Erbakan Street, No:19 Seydişehir/KONYA
ogok@erbakan.edu.tr

Mehmet KAYRICI, Assist Prof. Dr., PhD.
Necmettin Erbakan University, Seydişehir Vocational Scholl
Prof. Dr. Necmettin Erbakan Street, No:19 Seydişehir/KONYA
mkayrici@erbakan.edu.tr

Mehmet Turan DEMİRCİ, Assoc Prof. Dr., PhD.
Faculty of Technology
Selçuk University Alaeddin Keykubat Campus
Faculty of Technolgy PK:42075 Selçuklu / KONYA
turandemirci@selcuk@edu.tr